Modeling, Identification and Control, Vol. 45, No. 3, 2024, pp. 81–95, ISSN 1890–1328

Optimal Control Architecture for Balancing Performance and Cost in Oil and Gas Production Systems

Kushila Jayamanne, Bernt Lie

Department of Electrical Engineering, IT and Cybernetics, University of South-Eastern Norway, 3918 Porsgrunn, Norway. E-mail: {Kushila.R.Jayamanne, Bernt.Lie}@usn.no

Abstract

In the domain of process design, stakeholders pursue two interrelated yet potentially conflicting objectives: maximization of system performance and reduction of plant cost. The control architecture of a process not only determines the cost of the system, but also significantly influences its potential performance. Nevertheless, conventional processes for designing control architectures prioritize economic objectives while overlooking system performance. This paper introduces a systematic approach that integrates both these objectives simultaneously into the design of control architectures for oil and gas production systems. The method involves quantifying the trade-off between controllability, observability, and the cost associated with the control architecture. This quantification is posed as a multi-objective integer nonlinear programming problem, which is specified as a Pareto optimization problem. Solving this optimization problem yields a set of Pareto-optimal control architectures, enabling design engineers to explore optimal trade-offs between cost and performance. The efficacy of the proposed procedure is demonstrated through a real-world oil field example. Pareto-optimal architectures for the oil field are found using the developed framework. Subsequent analysis of the results reveals the indispensability of physical sensors for certain variables and the importance of well-balanced sensor distributions among the different wells in the oil field. To assess the impact of different architectures on closed-loop control performance, linear quadratic Gaussian (LQG) controllers are designed. Comparisons are made between the performance of LQG control systems instantiated on the identified Pareto-optimal architectures and non-optimal alternatives. This comparison highlights the pivotal role of optimal architectures in simultaneously enhancing performance and minimizing costs.

Keywords: Control architecture, Optimal design, Multi-objective optimization, Pareto optimal

1. Introduction

A fundamental part of control system design is determining the sensor-actuator configuration, i.e., the control architecture (Goodwin et al., 2001). To have complete knowledge and perfect control over a system, we would want to be able to directly measure every state using sensors and directly manipulate every state using actuators. However, due to practical limitations such as physical constraints, computational limitations, and cost considerations, achieving such complete control is usually not feasible; this is particularly true for large-scale systems like those encountered in the oil and gas industry. Thus, control architecture design requires strategic placement of only a limited number of sensors and actuators. The process of determining the appropriate number and location of these components for a system is known as control architecture design.

doi:10.4173/mic.2024.3.1

In the oil and gas industry, the conventional approach to control system design follows a sequential process. Initially, the control architecture is determined based on prior experience, primarily prioritizing budgetary constraints. Only once the control architecture is established does the focus shift towards achieving the desired performance. However, this approach overlooks a crucial aspect: the influence of control architecture on system performance. For instance, a poorly designed architecture could lead to unstable zero dynamics (e.g., time delays, inverse response), which may significantly limit the bandwidth of robust estimators and feedback controllers. Such performance limitations are impossible to overcome with subsequent controller or estimator design. Modifications may be necessary if a traditionally chosen architecture is implemented and fails to meet performance requirements. In oil and gas production applications, the cost of such modifications can be prohibitively high, making poor choices of control architecture unacceptable. Thus, it is essential to acknowledge the interplay between control architecture and system performance, and consequently incorporate both system performance and economic considerations into the control architecture design process.

The optimal control architecture problem has been extensively explored in various fields, such as flexible structures (Hiramoto et al., 2000; Hać and Liu, 1993; Darivandi et al., 2013), chemical engineering (Kookos and Perkins, 1999; Antoniades and Christofides, 2000), power systems engineering (Summers and Lygeros, 2014; Munz et al., 2014), and others. The literature includes a number of articles that specifically consider the multiple objectives of system performance and cost-effectiveness. For example, Luyben and Floudas (1994) propose a method to simultaneously evaluate economic and open-loop controllability objectives in process synthesis. This approach transforms the problem into a multi-objective mixed-integer nonlinear programming (MINLP) problem. The set of trade-off solutions is identified through the ε-constraint method, while the cutting-plane algorithm identifies the best compromise solution. Application of the method is demonstrated on a binary distillation column. Similarly, Muske and Georgakis (2003) address sensor placement in process synthesis, aiming to optimize process information while minimizing sensor costs. The trade-off is formulated as a Pareto optimization problem. A continuous stirred tank reactor (CSTR) example is used for demonstration. In another study, Sen et al. (2016) investigate sensor placement in an IGCC power plant with three objectives: minimizing cost, maximizing observability, and maximizing plant efficiency. A novel algorithmic framework is developed to identify the Pareto solutions. Lastly, Cha et al. (2012) employ a multi-objective genetic algorithm (MOGA) to address structural control under seismic excitation. The MOGA balances control cost and performance, providing diverse control architectures for benchmark building structures.

Despite the substantial research in control architecture design, to our knowledge, there are no studies focusing on its application in the oil and gas industry. This work aims to address this gap by laying the foundation for an optimal control architecture framework tailored to oil and gas production plants. Our primary objective is to consider the multiple objectives of system performance and equipment cost in designing the control architecture. To achieve this, we will draw upon relevant methodologies, objective functions, and optimization techniques from existing literature and adapt them to suit the specific requirements of oil and gas production plants. The resulting customized framework will pave the way for potential future enhancements and refinements. We will also apply the framework to address a real-world problem within the oil industry, evaluating its efficacy in addressing industry-specific challenges.

The paper is organized as follows. In Section 2, we present a systematic framework to achieve the desired architecture for oil and gas production system. This includes details of the process model used for analyzing control performance, the metrics chosen for evaluating system performance and cost, and the numerical computation approach employed to solve the architecture problem. In Section 3, we utilize a real-world gas-lifted oil field as a case study to demonstrate the practical application of our architecture design procedure. We demonstrate how the optimal architecture for the oil field is identified, and subsequently design a complete control system based on the identified architectures. Additionally, we provide a detailed analysis of the system's closed-loop performance. In Section 4, we engage in a discussion of the limitations of our control architecture design procedure. Finally, in Section 5, we provide a summary of the key findings, contributions, and avenues for future research.

2. Control Architecture Design Framework

2.1. Process Model

The use of a linearized model for control architecture design offers a simpler and more efficient approach compared to using a nonlinear model. This approach also benefits from the availability of well-established linear techniques for linear plant models. As a result,

it is widely adopted for control architecture selection in the existing literature. Particularly for nonlinear systems that operate in close proximity to equilibria, which is often the case for oil/gas production systems, linear methods are highly applicable. Therefore, we choose to employ a linearized plant model for designing optimal control architecture. We will specifically focus on linear, time-invariant dynamic models, where the system dynamics are described by the state-space representation in eq. (1) below.

$$\begin{aligned} \dot{x}(t) &= Ax(t) + Bu(t) \\ y(t) &= Cx(t) + Du(t)\,. \end{aligned} \tag{1}$$

Here, $x(t) \in \mathbb{R}^n$ is the state vector; $u(t) \in \mathbb{R}^p$ is the input vector; $y(t) \in \mathbb{R}^q$ is the output vector; $A \in \mathbb{R}^{n\times n}$ is the system matrix; $B \in \mathbb{R}^{n\times p}$ is the input matrix; $C \in \mathbb{R}^{q\times n}$ is the output matrix; and $D \in \mathbb{R}^{q\times p}$ is the feedforward matrix.

2.2. System Performance Metric

In our methodology, we recognize that a controller designed based on a simplified model at the design stage does not necessarily ensure the desired performance during the operational stage. Therefore, we choose to utilize open-loop performance measures — a common practice in existing literature. By doing so, our approach becomes independent of the specific details of the controller design, a quality that is generally deemed desirable (Van De Wal and De Jager, 2001), for reasons of efficiency and to ensure unbiased conclusions regarding the viability of the architecture under different scenarios.

We will specifically focus on observability and controllability as the key system properties of interest. Observability refers to the ability to estimate or observe the system's internal states based on available sensor measurements. Controllability, on the other hand, pertains to the ability to steer the system's state from any initial condition to a desired state using actuators. A highly controllable system enables precise manipulation of the system's behavior, while a highly observable system facilitates accurate state estimation, even in the presence of uncertainties or disturbances. Hence, focusing on observability and controllability during sensor and actuator selection, allows for greater flexibility and effectiveness in controller design, enabling control designers to shape the system's behavior, stabilize unstable systems, and meet specific performance requirements. These properties have been extensively employed in the control architecture design literature (Georges, 1995; Lim, 1992; Hać and Liu, 1993; Leleu et al., 2000; Bruant et al., 2010; Summers and Lygeros, 2014; Pequito et al., 2016; Li et al., 2015; Manohar et al., 2022), further supporting their significance.

The concepts of controllability and observability are binary in nature, however the Gramians associated with them provide an energy-related quantitative measure. The observability Gramian $W_\mathrm{o}(t_\mathrm{f})$ and the controllability Gramian $W_\mathrm{c}(t_\mathrm{f})$ over a specified time horizon t_f are given by the following equations:

$$\begin{aligned} W_\mathrm{o}(t_\mathrm{f}) &= \int_0^{t_\mathrm{f}} e^{A^T t} C^T C e^{At}\,, \quad dt \in \mathbb{R}^{n\times n}\,, \\ W_\mathrm{c}(t_\mathrm{f}) &= \int_0^{t_\mathrm{f}} e^{At} B B^T e^{A^T t}\,, \quad dt \in \mathbb{R}^{n\times n}\,. \end{aligned} \tag{2}$$

For stable systems, the infinite-horizon (i.e., $t_\mathrm{f} \to \infty$) observability Gramian W_o and controllability Gramian W_c can be found by solving the following algebraic Lyapunov equations:

$$\begin{aligned} A^T W_\mathrm{o} + W_\mathrm{o} A + C^T C &= 0\,, \\ A W_\mathrm{c} + W_\mathrm{c} A^T + B B^T &= 0\,. \end{aligned} \tag{3}$$

We will concentrate on the infinite-horizon Gramians owing to their ease of computation. Nevertheless, it is important to note that the finite-horizon Gramian can also be used. The main drawback of using the finite-horizon Gramians is that one must evaluate eq. (2) instead of eq. (3), which might be more challenging. However, an advantage of the finite-horizon Gramians is their applicability to unstable systems.

The Gramians are positive semidefinite matrices. Various scalar metrics can be used to quantify the "size" of the Gramians, including the minimum eigenvalue, determinant, and trace (Müller and Weber, 1972). For our purposes, we will focus on the minimum eigenvalue metric $\underline{\lambda}$. The objectives for sensor selection and actuator selection, utilizing the minimum eigenvalues, are as follows.

- Sensor selection objective:

$$\max \underline{\lambda}\left(W_\mathrm{o}(C, A)\right)\,. \tag{4}$$

- Actuator selection objective:

$$\max \underline{\lambda}\left(W_\mathrm{c}(A, B)\right)\,. \tag{5}$$

The underlying physical idea behind these objective functions is to minimize the input energy required to reach a given state and to maximize the output energy generated by a given state. A more detailed explanation is provided by Georges (1995).

Apart from controllability and observability, various other performance criteria have also been employed in the control architecture design literature; see,

for example, the survey paper by Van De Wal and De Jager (2001) for an excellent overview of these criteria. Within the current framework, these metrics can be employed in different ways: they can either substitute the performance metrics in eqs. (4) and (5), or they can be incorporated as supplementary objectives or constraints in the multi-objective optimization problem.

2.3. Cost Metric

We introduce scalar metrics to quantify the cost associated with the sensors and actuators. For the sensor cost, we define the metric as

$$e_{\mathrm{s}}^{T}\delta_{\mathrm{s}}\,. \tag{6}$$

Here, $e_{\mathrm{s}} = \left[e_{\mathrm{s}}^{1}, e_{\mathrm{s}}^{2}, \cdots, e_{\mathrm{s}}^{q}\right]^{T}$ is a vector containing the sensor expense for measuring each physical property represented by the system outputs, $y = [y_1, y_2, \cdots, y_q]$. The sensor expense may encompass the capital cost as well as the present value of anticipated future operating cost, including maintenance costs, whether on a relative or absolute basis. The binary vector $\delta_{\mathrm{s}} = \left[\delta_{\mathrm{s}}^{1}, \delta_{\mathrm{s}}^{2}, \cdots, \delta_{\mathrm{s}}^{q}\right] \in \{0,1\}^{q}$ in eq. (6) represents the design variable; each element δ_{s}^{i} is assigned a value of 1 if a sensor is placed at location i, and 0 otherwise.

Likewise, we also define a scalar metric for the actuator cost:

$$e_{\mathrm{a}}^{T}\delta_{\mathrm{a}}\,. \tag{7}$$

In this case, $e_{\mathrm{a}} = \left[e_{\mathrm{a}}^{1}, e_{\mathrm{a}}^{2}, \cdots, e_{\mathrm{a}}^{p}\right]^{T}$ represents a vector containing the actuator expense for controlling each physical property represented by the system inputs $u = [u_1, u_2, \cdots, u_p]$. The binary vector $\delta_{\mathrm{a}} = \left[\delta_{\mathrm{a}}^{1}, \delta_{\mathrm{a}}^{2}, \cdots, \delta_{\mathrm{a}}^{p}\right] \in \{0,1\}^{p}$ in eq. (7) is the design variable; each element δ_{a}^{i} is assigned a value of 1 if an actuator is placed at location i, and 0 otherwise.

2.4. Numerical Computation

Multi-objective optimization involves the simultaneous optimization of individual objectives. Rather than seeking a single optimal solution, it aims to discover a collection of solutions known as Pareto optimal solutions. These solutions define a boundary beyond which improving any objective would necessitate sacrificing at least one other objective. The set of Pareto optimal solutions provides decision-makers with a range of trade-off options to choose from, enabling well-informed decision-making.

Various techniques exist for generating Pareto optimal solutions. Traditional approaches include the weighted sum method, the goal programming method, ε-constraint method, and genetic algorithms (GAs). Among these, GAs, in particular, are widely utilized in control architecture literature (Milosevic and Begovic, 2003; Flynn and Todd, 2010; Cha et al., 2012). They efficiently explore diverse solutions without requiring derivatives, making them advantageous for handling non-linear problems. However, GAs can be computationally expensive and require careful parameter tuning to achieve optimal performance. Despite these limitations, when used judiciously, GAs are powerful tools for generating the Pareto set, making them well-suited for our work. In instances where GAs might be insufficient, especially for large-scale problems, modern machine learning techniques emerge as promising alternatives. Recent studies on optimal control architecture (Manohar et al., 2018; Semaan, 2017; Paris et al., 2023) delve into the utilization of machine learning techniques, revealing their efficacy in successfully tackling large problems. However, our specific focus on GAs aligns with the scale and requirements of our current work.

The following describes the steps through which a GA finds the Pareto front for the control architecture problem:

- In a GA, each potential sensor/actuator configuration would be referred to as an individual or chromosome. The configurations would be encoded as binary strings, with each element corresponding to the presence or absence of a sensor/actuator at a specific location.

- The algorithm begins by randomly generating an initial population of individuals. Over subsequent generations, this population evolves toward better solutions. In each generation, the fitness of every individual in the population is evaluated based on the defined objectives, i.e., system performance and cost.

- The selection process follows, favoring individuals with higher fitness as parents for the next generation. There are different selection methods available, such as roulette wheel selection or tournament selection, which simulate the survival-of-the-fittest principle. These methods ensure that individuals with superior fitness contribute more genetic material to the next generation.

- Next, genetic operators like crossover and mutation are applied to the selected parents to generate new offspring. The newly created offspring replace a portion of the population, typically the least fit individuals, thereby propelling the population towards improved sensor/actuator configurations that optimize the multiple objectives.

- By iteratively applying these steps, the genetic algorithm explores the space of possible sensor configurations, favoring better-performing solutions and gradually converging towards a set of optimal or near-optimal placements that offer a trade-off between the multiple objectives.

- The algorithm runs until a termination criterion is met, such as a maximum number of generations, desired fitness level, or predefined computational budget. The final population consists of a diverse set of solutions, known as the Pareto front or Pareto-optimal solutions, representing the best compromises between the conflicting objectives.

For more in-depth information on GAs, consult the available literature. Notable sources include Mitchell (1998) and Goldberg (1989).

3. Illustrative Example

In this section, we will use an example of a gas-lifted oil field to demonstrate the application of the architecture design procedure.

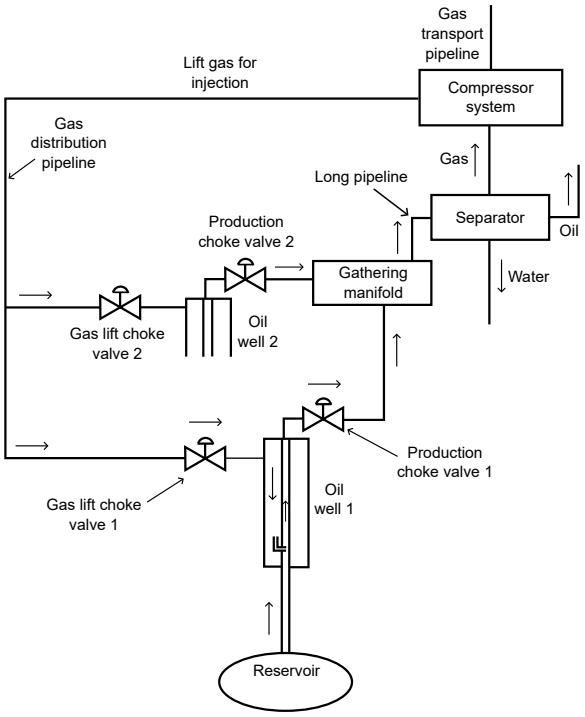

Figure 1: Schematic of the oil field adapted from Sharma et al. (2011)

3.1. Gas-Lifted Oil Field Model

A model of a gas-lifted oil field consisting of five oil wells, which has been validated against data from a real oil field, is proposed by Sharma et al. (2011). Jayamanne (2021) subsequently presents an adapted version of this model, focusing on two oil wells. Figure 1 illustrates a possible architecture for this system. A compressor releases pressurized lift-gas into a shared pipeline for distribution among oil wells. The gas enters the well's annulus through a gas-lift choke valve. From there, it is injected into the tubing at an optimal depth through a one-way gas injection valve. Mixing with reservoir oil, the gas reduces its density, lowering the hydrostatic pressure in the tubing and consequently the bottom hole pressure. This increased differential pressure drives the liquid column upward. The resulting mixture exits through a production choke valve, collects in a common gathering manifold, and is transported to a separator for constituent separation. The separated gas is recycled back to the compressor system for reuse in the lifting process.

The system is mathematically described by a differential-algebraic system of equations (DAE). The equations encompass mass balances for state variables and algebraic equations for valve characteristics, pressures, average densities, and other parameters. The model focuses on the flow dynamics of the wells, from the gas-lift choke valve up to the production choke valve. Dynamics related to the gas distribution manifold, gathering manifold, separator, etc., are omitted. Additionally, the model is based on several simplifying assumptions:

- Temperature remains constant for both lift gas and multiphase fluid across all sections of the wells.

- Compressibility factor of the lift gas is constant.

- Reservoir pressure is constant.

- Only oil is produced from the reservoir.

- The two phases of the multiphase fluid in the tubing are evenly distributed (i.e., homogeneous mixture).

- There is no slip between the two phases.

- There are no frictional losses in the pipelines.

For the sake of our work, we linearized the DAE system around a selected operating point using symbolic differentiation in Julia. The `linearize` function from the ModelingToolkit package (Ma et al., 2021) was used for this. The resulting linear model may be written in

state space form as

$$\begin{aligned} \dot{x} &= Ax + Bu \\ y &= Cx + Du\,, \end{aligned} \tag{8}$$

where

$$\begin{aligned} x &= \left[m^1_{\text{ga}}, m^1_{\text{gt}}, m^1_{\text{ot}}, m^2_{\text{ga}}, m^2_{\text{gt}}, m^2_{\text{ot}}\right]\,, \\ u &= \left[w^1_{\text{ga}}, C^1_{\text{v}}, w^2_{\text{ga}}, C^2_{\text{v}}\right]\,, \\ y &= \left[P^1_{\text{a}}, P^1_{\text{ainj}}, P^1_{\text{tinj}}, P^1_{\text{wh}}, w^1_{\text{ginj}}, w^1_{\text{gop}},\right. \\ &\quad \left. P^2_{\text{a}}, P^2_{\text{ainj}}, P^2_{\text{tinj}}, P^2_{\text{wh}}, w^2_{\text{ginj}}, w^2_{\text{gop}}\right]\,. \end{aligned}$$

There are six states in total, with three states associated with each of the two wells (denoted as i): mass of lift-gas in the annulus m^i_{ga}, mass of lift-gas in the tubing above the injection point m^i_{gt}, and mass of oil in the tubing above the injection point m^i_{ot}. There are four potential manipulated input variables: mass flow rate of gas through the gas-lift choke valve w^i_{ga}, and production choke valve characteristic C^i_{v} (which is a function of its opening u^i_2). Furthermore, we consider twelve potential measured variables: pressure downstream of the gas-lift choke valve P^i_{a}, pressure upstream of the gas injection valve P^i_{ainj}, pressure downstream of the gas injection valve P^i_{tinj}, pressure upstream of the production choke valve P^i_{wh}, mass flow rate of gas injected into the tubing w^i_{ginj}, mass flow rate of the mixture of gas and oil through the production choke valve w^i_{gop}.

To ensure accurate assessments of the controllability and observability measures, it is essential to consider the impact of scaling on these quantities. Here, we adopt the scaling procedure proposed by Skogestad and Wolff (1996) to normalize the system. It involves normalizing the variables with respect to their maximum allowed/expected range. This procedure assures that both the outputs and inputs have comparable magnitudes by restricting the variables to be within the range of -1 to +1.

The normalized linear model — which we will use in our control architecture study — also can be represented by eq. (8). The matrices A, B, C, and D for this model are provided in Appendix A, along with additional information on the linearization process.

3.2. Optimal Control Architecture: Problem

In our study, we will treat the problems of sensor selection and actuator selection as two separate problems for the sake of simplified analysis. However, it is important to note that they can also be viewed as a unified problem. The results will be the same since there are no interactions between the two problems in our specific example.

We have two trade-off objectives, given in eqs. (9) and (10), for the sensor selection problem.

$$J_1 = \max_{\delta_{\text{s}} \in \{0,1\}^q} \underline{\lambda}\left(W_{\text{o}}\left(\delta_{\text{s}}\right)\right)\,, \tag{9}$$

$$J_2 = \min_{\delta_{\text{s}} \in \{0,1\}^q} e_{\text{s}}^T \delta_{\text{s}}\,. \tag{10}$$

Here, the binary vector $\delta_{\text{s}} = \left(\delta^1_{\text{s}}, \delta^2_{\text{s}}, \cdots, \delta^q_{\text{s}}\right) \in \{0,1\}^q$ is our design variable; $q = 12$ is the number of candidate sensors. Its elements δ^i_{s} take on the value 1 if a sensor is placed at location i or the value 0 if it is not used. J_1 is the cost function that quantifies the degree of observability; it is a function of the observability gramian W_{o}. J_2 is a pseudo-economic objective function in terms of the relative costs of placing sensors $e_{\text{s}} = \left(e^1_{\text{s}}, e^2_{\text{s}}, \cdots, e^{n_{\text{s}}}_{\text{s}}\right) \in \{1,2,3\}^q$. Elements e^i_{s} are integer variables that can take the values 1, 2, or 3, indicating low-cost, medium-cost and high-cost sensors, respectively. (Note: In this study, the exact monetary costs were unavailable, hence we use a relative cost description.) Table 1 provides the relative cost associated with each potential sensor.

Likewise, we have two trade-off objectives, given in eqs. (11) and (12), for the actuator selection problem.

$$J_3 = \max_{\delta_{\text{a}} \in \{0,1\}^p} \underline{\lambda}\left(W_{\text{c}}\left(\delta_{\text{a}}\right)\right)\,, \tag{11}$$

$$J_4 = \min_{\delta_{\text{a}} \in \{0,1\}^p} e_{\text{a}}^T \delta_{\text{a}}\,. \tag{12}$$

Here, the binary vector $\delta_{\text{a}} = \left(\delta^1_{\text{a}}, \delta^2_{\text{a}}, \cdots, \delta^p_{\text{a}}\right) \in \{0,1\}^p$ is our design variable; $p = 4$ is the number of candidate actuators. Its elements δ^i_{a} take on the value 1 if an actuator is placed at location i or the value 0 if it is not placed. J_3 is the cost function that quantifies the degree of controllability; it is a function of the controllability gramian W_{c}. J_4 is a pseudo-economic objective function in terms of the relative costs of placing actuators $e_{\text{a}} = \left(e^1_{\text{a}}, e^2_{\text{a}}, \cdots, e^p_{\text{a}}\right) \in \{1,2,3\}^p$. Elements e^i_{a} are integer variables that can take the values 1, 2, or 3, indicating low-cost, medium-cost and high-cost actuators, respectively. Table 1 provides the relative cost associated with each potential actuator.

3.3. Optimal Control Architecture: Solution

To perform optimization we use the `gamultiobj` function in MATLAB, which finds the Pareto front of multiple fitness functions using GA. We apply it separately for the sensor selection problem (i.e., for objectives J_1 and J_2) and for the actuator selection problem (i.e., for objectives J_3 and J_4). In both cases, we run the GA for 100 generations with a population size of 250 and a crossover proportion of 0.8.

Table 1: Costs of sensors and actuators.

	Variable	Relative cost
Sensors	P_{a}	1
	P_{ainj}	2
	P_{tinj}	2
	P_{wh}	1
	w_{ginj}	3
	w_{gop}	3
Actuators	w_{ga}	2
	C_{v}	3

Since the number of sensors and actuators in our specific example is moderate, it is possible to determine the objective values for all possible configurations of sensors and actuators. Therefore, we undertake this analysis as well. This will serve two purposes: firstly, it will allow us to verify whether `gamultiobj` has converged to the true optimal solutions, and secondly, it will provide additional insights into the problem itself (discussion in Section 3.4).

Figure 2 displays the Pareto front found for the sensor problem as well as all other possible non-optimal sensor configurations (i.e., dominated solutions), while Figure 3 illustrates the same for the actuator problem.

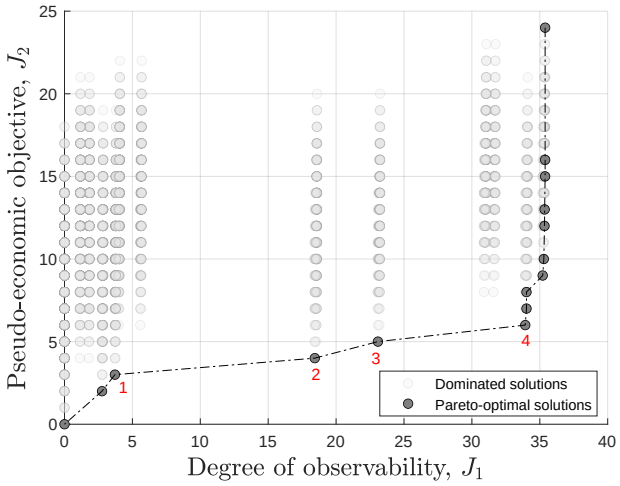

Figure 2: Pareto front for sensor selection

It is evident from Figure 2 that `gamultiobj` has indeed converged to the true optimal solutions. Despite allowing for a large number of sensors, the Pareto front for the sensor problem consists of only 15 sensor configurations out of a maximum of 4096. The results reveal that increasing the sensor budget has a positive impact on observability up to a threshold of approximately 35; see abscissa of Figure 2. Beyond the point indicated by "4" in Figure 2, the Pareto front exhibits a steep slope, indicating that achieving marginal improvements in observability comes at a higher cost.

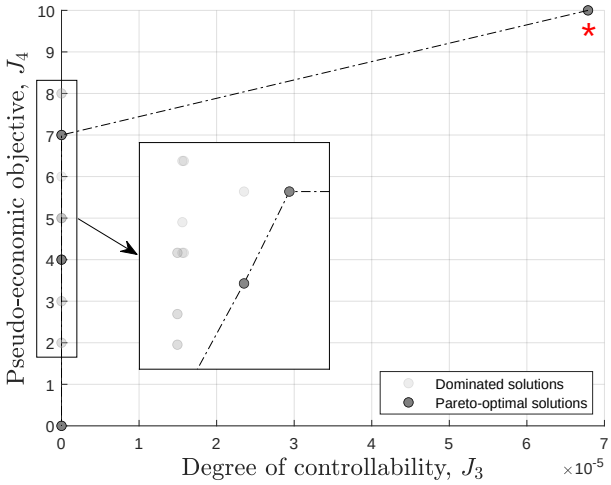

Figure 3: Pareto front for actuator selection

Similarly, for the actuator problem, it is seen from Figure 3 that `gamultiobj` has converged to the true optimal solution. The Pareto front consists of only 4 actuator configurations out of a possible 16. Among these configurations, three form a cluster, providing similar levels of controllability at varying costs. The fourth configuration (indicated by the red * in Figure 3), involves the actuation of all four potential input variables. This configuration provides significantly higher controllability but comes at a higher cost.

The optimal sensor configurations corresponding to the Pareto front in Figure 2 are provided in Table 2. This table provides some valuable insights into the sensor selection problem. Notably, it reveals that variables P_{tinj} and P_{wh} are present in nearly all optimal solutions. This indicates the indispensability of physical sensors for monitoring these particular variables. The solutions labeled "1", "2", "3", and "4" in Figure 2 further support this finding: they demonstrate significant improvements in observability when transitioning from having sensors solely for measuring P_{wh} of both wells (i.e., solution "1"), to including sensors for both P_{wh} and P_{tinj} of both wells (i.e., solution "4"). Moreover, Table 2 shows that all optimal sensor configurations involve sensors for both wells, which is expected considering the need for comprehensive monitoring. However, a noteworthy observation is that a greater number of sensors are consistently allocated to Well2, particularly in the solutions following "4" in Figure 2. This allocation pattern may be influenced by factors such as the productivity index of Well1 being greater than that of

Table 2: Pareto-optimal sensor configurations.

Objective		No. of	Candidate sensor											
			Well1						Well2					
J_1	J_2	sensors	P^1_{a}	P^1_{ainj}	P^1_{tinj}	P^1_{wh}	w^1_{ginj}	w^1_{gop}	P^2_{a}	P^2_{ainj}	P^2_{tinj}	P^2_{wh}	w^2_{ginj}	w^2_{gop}
0	0	0	0	0	0	0	0	0	0	0	0	0	0	0
2.76	2	2	0	0	0	1	0	0	0	0	0	1	0	0
3.71	3	2	0	0	0	1	0	0	0	0	1	0	0	0
18.4	4	2	0	0	1	0	0	0	0	0	1	0	0	0
23.1	5	3	0	0	1	0	0	0	0	0	1	1	0	0
34.0	6	4	0	0	1	1	0	0	0	0	1	1	0	0
34.0	7	5	0	0	1	1	0	0	1	0	1	1	0	0
34.0	8	6	1	0	1	1	0	0	1	0	1	1	0	0
35.2	9	5	0	0	1	1	0	0	0	0	1	1	0	1
35.3	10	6	0	0	1	1	0	0	1	0	1	1	0	1
35.3	12	7	0	0	1	1	0	0	1	1	1	1	0	1
35.4	13	7	0	0	1	1	0	0	1	0	1	1	1	1
35.4	15	8	0	0	1	1	0	0	1	1	1	1	1	1
35.4	16	9	1	0	1	1	0	0	1	1	1	1	1	1
35.4	24	12	1	1	1	1	1	1	1	1	1	1	1	1

Well2; it is possible that assigning a greater number of sensors to Well2 addresses its comparatively lower productivity and enable more precise control and monitoring.

Table 3: Pareto-optimal actuator configurations.

Objective		No. of	Candidate actuator			
			Well1		Well2	
J_3	J_4	sensors	w^1_{ga}	C^1_{v}	w^2_{ga}	C^2_{v}
0	0	0	0	0	0	0
$1.75e^{-9}$	4	2	1	0	1	0
$2.95e^{-9}$	7	3	1	1	1	0
$6.79e^{-5}$	10	4	1	1	1	1

Table 3, which lists the optimal actuator configurations corresponding to the Pareto front in Figure 3, reveals similar observations regarding actuator selection. Most notable is that variable w_{ga} is consistently selected across all solutions. This highlights the significance of actuation in relation to this specific variable.

3.4. Impact of Control Architecture on Closed-Loop Control Performance

In our approach, identification of all possible trade-off architectures enables design engineers to explore and choose optimally between performance and cost. Engineers could, for example, design a controller for any identified architecture and assess its closed-loop response through simulations. These simulations could reveal potential sacrifices in closed-loop performance linked to control equipment cost.

In the following, we illustrate how optimal trade-offs may be explored: we will design and analyze the performance of closed-loop control systems for selected sensor and actuator configurations. Our chosen methodology for this task is linear quadratic Gaussian/loop transfer recovery (LQG/LTR), with settling time as the specific closed-loop performance metric of interest.

In LQG control, the plant is assumed to have the form in eq. (13) below.

$$\begin{aligned} \dot{x} &= Ax + Bu + w \\ y &= Cx + Du + v\,. \end{aligned} \tag{13}$$

Here, w denotes process noise and v represents measurement noise. The LTR procedure involves the following steps:

- Assuming state feedback, we define the linear–quadratic regulator (LQR) control problem with the cost function in eq. (14) below.

$$J = \int_0^\infty \left(x^T Q x + u^T R u\right) dt\,. \tag{14}$$

  Here, Q is the state weighting matrix and R is the control weighting matrix. We set $Q = C^T C$ and $R = \rho I$, where ρ is a scalar. Then, the value of ρ is adjusted to find the controller gain K that gives a desirable loop transfer function $K\phi(s)B$ (where

$\phi(s) = (sI - A)^{-1}$); the singular value plots of $K\phi(s)B$ are examined to ensure that it satisfies the desired performance criteria.

- When the singular values of $K\phi(s)B$ are deemed satisfactory, a Kalman filter is introduced with process noise covariance matrix W and measurement noise covariance matrix V. We set $W = BB^T$ — a commonly used simplification that implies w enters the system through the control inputs — and $V = \mu I$, where μ is a scalar. Then, loop transfer recovery is achieved by adjusting the value of μ to find the Kalman gain L. This adjustment aims to make the LQG loop transfer function $G(s)C_{\text{LQG}}$ approximately equal to the desired loop transfer function $K\phi(s)B$. (Here, $G(s) = C\phi(s)B$ is the plant transfer function and $C_{\text{LQG}} = K\left(sI - A + BK + LC\right)^{-1}L$ is the LQG controller transfer function.) As μ tends to zero $G(s)C_{\text{LQG}}$ will tend to $K\phi(s)B$. To assess the degree of match between the two loop transfer functions, the singular value plots of both are plotted in the same plot. The tuning parameters μ and ρ are iterated upon until a system that is as fast as possible is achieved while still having overlap.

For a more detailed understanding of the recovery procedure, we suggest consulting the original publications by Doyle and Stein (1979, 1981), and the tutorial paper by Stein and Athans (1987).

We will begin by examining the impact of different sensor configurations on feedback control performance. Specifically, we will focus on three sensor configurations: sConfig1, representing the non-optimal configuration $[1,0,0,0,0,0,1,1,1,1,0,1]$; sConfig2, representing the Pareto-optimal configuration $[0,0,1,1,0,0,1,0,1,1,0,1]$; and sConfig3, representing the Pareto-optimal configuration $[1,1,1,1,1,1,1,1,1,1,1,1]$. Both sConfig1 and sConfig2 have an equal number of sensors and incur the same pseudo-economic cost of $J_2 = 10$. However, sConfig1 exhibits significantly lower observability with a value of $J_1 = 8.37e^{-9}$ compared to sConfig2's observability of 35.3. On the other hand, sConfig2 and sConfig3 have similar degrees of observability, but sConfig3 incurs more than double the cost of sConfig2, specifically $J_2 = 24$.

We will employ LQG/LTR controllers for each sensor configuration, while using a common Pareto-optimal actuator configuration $[1,0,1,0]$. Following the aforementioned LTR procedure, we select tuning parameters $\rho = 1$ and $\mu = 0.01$ for sConfig3 found by trial-and-error. For sConfig1 and sConfig2, we assume the same LQG controller tunings. This assumption implies that the ratio between input effort minimization and state deviation attenuation, as well as the ratio between process noise covariance and measurement noise covariance, remains the same for all three configurations.

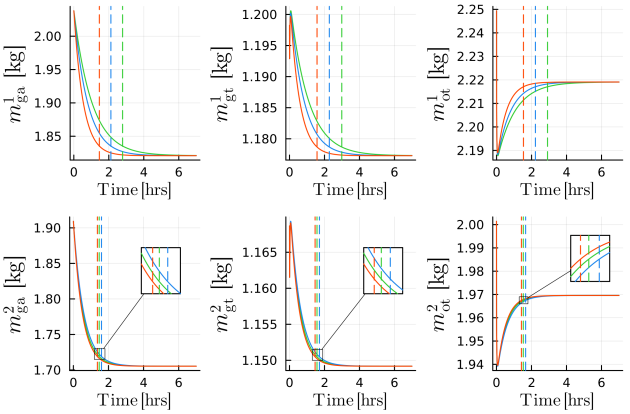

Figure 4: State response of LQG control to a disturbance (green: sConfig1; blue: sConfig2; red: sConfig3)

Figure 4 illustrates the response and settling times for each system when subjected to a state disturbance of $[0.3, 0.3, 0.3, 0.3, 0.3, 0.3]$ (Note: This is the normalized value of the disturbance. The corresponding actual state is $[2.04, 1.20, 2.25, 1.91, 1.17, 2.00]$.) when at operating point. Table 4 lists the settling times. The figure reveals that the responses of Well2 are nearly identical across all three sensor configurations. This is reasonable as they share four common sensors, including those for monitoring the key variables that contribute more to the controllability, as identified in Sec. 3.3, namely P_{tinj} and P_{wh}. However, upon closer examination, slight differences emerge. Notably, sConfig1, the non-optimal configuration, exhibits a slightly faster response compared to the optimal sConfig2. This difference can be attributed to the presence of an additional sensor in sConfig1 for measuring P_{ainj}. Similarly, sConfig3 shows a slightly faster response than sConfig2 due to the inclusion of an extra sensor for measuring w_{ginj}.

In contrast, the responses of Well1 differ significantly across the sensor configurations. The response of sConfig1 noticeably lags behind sConfig2. This can be attributed to sConfig1 having only one sensor for monitoring Well1, and it is neither dedicated to measuring P_{tinj} nor P_{wh}. This observation highlights the importance of adopting an optimal sensor configuration, which can result in superior control performance while keeping the sensor cost unchanged. While this finding is intuitive in the present example due to the well-balanced sensors in sConfig2 and the lack of such balance in sConfig1, in a more complex process, recogniz-

Table 4: LQG controller settling times for different sensor configurations.

	State variable	Settling time [hrs] sConfig1	sConfig2	sConfig3
Well1	m^1_{ga}	2.79	2.12	1.46
	m^1_{gt}	2.99	2.28	1.57
	m^1_{ot}	2.91	2.22	1.54
Well2	m^2_{ga}	1.47	1.60	1.37
	m^2_{gt}	1.57	1.71	1.46
	m^2_{ot}	1.53	1.67	1.43

ing and considering such observations can prove to be invaluable.

When comparing between the two optimal configurations, while sConfig3 performs better than sConfig2, the improvement achieved is comparable to the difference observed between sConfig1 and sConfig2. This is interesting because sConfig2 only utilizes two sensors — dedicated to measuring the two important variables — whereas sConfig3 has all six possible sensors. This suggests that adding extra sensors beyond those contributing significantly to controllability does not yield substantial performance gains.

Next, we will analyze how different actuator configurations impact closed-loop control performance. As observed in Section 3.3 all actuator configurations, except one, exhibited similar controllability levels. The exceptional configuration, which we will refer to as aConfig1, represented by $[1, 1, 1, 1]$, i.e., actuating all four potential input variables, demonstrated relatively higher controllability. We will compare its performance with the Pareto-optimal configuration represented by $[1, 0, 1, 0]$, which we will refer to as aConfig2. The observability values for aConfig1 and aConfig2 were $J_3 = 6.79e^{-5}$ and $J_3 = 1.75e^{-9}$, respectively. Additionally, aConfig1 incurs a pseudo-economic cost of $J_4 = 10$, which is more than double the cost of aConfig2, which is 4.

Table 5: LQG controller settling times for different actuator configurations.

	State variable	Settling time [hrs] aConfig1	aConfig2
Well1	m^1_{ga}	1.56	1.46
	m^1_{gt}	1.54	1.57
	m^1_{ot}	1.56	1.54
Well2	m^2_{ga}	1.48	1.37
	m^2_{gt}	1.46	1.46
	m^2_{ot}	1.48	1.43

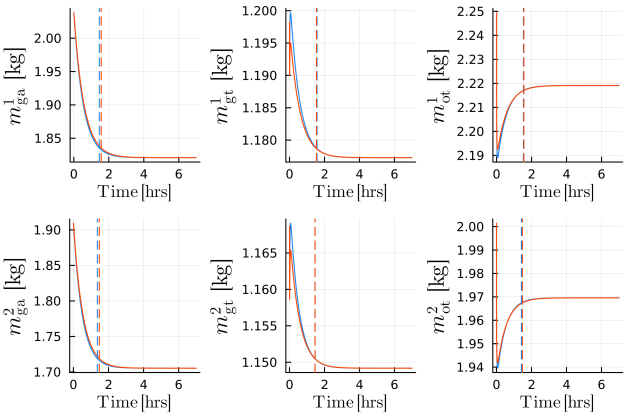

Figure 5: State response of LQG control to a disturbance (red: aConfig1; blue: aConfig2)

To create LQG controllers, we will employ the Pareto-optimal sensor configuration sConfig3 from before with aConfig1 and aConfig2. The same controller parameters $\rho = 1$ and $\mu = 0.01$ as before will be used for both architectures. Figure 5 illustrates the response of the states and settling times for each system, when subjected to the same initial state disturbance, $[0.3, 0.3, 0.3, 0.3, 0.3, 0.3]$, as in the sensor configuration case. Table 5 presents the settling times.

Interestingly, the state responses for both actuator configurations are nearly identical. This implies that introducing actuators to control C_v in addition to w_{ga} does not expedite the system's response. One potential explanation is that although aConfig1 demonstrates high controllability, it is only *relatively higher* compared to other possible actuator configurations; in absolute terms, the controllability values for all configurations are nearly zero. Consequently, we can not draw any definitive conclusions regarding the impact of different actuator configurations on the closed-loop performance in this scenario.

It is important to note that the closed-loop simulations presented above do not generalize open-loop observability and controllability measures; instead, they reveal sacrifices in our chosen closed-loop performance metric — settling time — associated with changes in control equipment cost.

4. Discussion

In our approach to control architecture design, we have prioritized controllability and observability as the key performance criteria. Although these properties are generally considered desirable, it is important to note that there is no guarantee that good control can be achieved even if all states are controllable and observ-

able. For instance, there may be bandwidth limitations that cannot be found by studying the Gramians.

One well-known limitation is the presence of a right half-plane (RHP) zero in the plant transfer function, which restricts the achievable bandwidth regardless of the controller used (Lie, 1995). While an RHP zero exhibits a 20 dB/decade rising gain magnitude like a conventional zero, it introduces a 90° phase lag instead of a lead. Compensating for this characteristic is challenging, if not impossible. As a result, the designer is often compelled to decrease the loop gain at a relatively low frequency. Consequently, the crossover frequency may be significantly lower than it could be, leading to a substantial degradation in dynamic response.

To illustrate this issue, consider the example transfer function with two inputs given in eq. (15) below.

$$y = \frac{(1-2s)}{(1+4s)\,(1+5s)}u_1 + \frac{(1+2s)}{(1+4s)\,(1+5s)}u_2\,. \quad (15)$$

When selecting the optimal input based on controllability, we find that input u_1, which introduces an RHP zero to the system, is chosen: $J_3 = 0.1249$ for u_1, while $J_3 = 0.0041$ for u_2. However, we can demonstrate why u_1 is not the ideal choice in this case by tuning a proportional-integral (PI) controller for each input.

We will refer to the system using u_1 as "sys1" and the system using u_2 as "sys2". We use the `pidtune` function in MATLAB for automatic PI controller tuning. The resulting PI controller parameters for sys1 are $K_\mathrm{p} = 1.13$ and $K_\mathrm{i} = 0.122$, while for sys2, they are $K_\mathrm{p} = 1.49$ and $K_\mathrm{i} = 0.442$. Here, K_p represents the proportional gain, and K_i represents the integral gain. The step responses of the two PI control systems are depicted in Figure 6. The inverse response exhibited by sys1 is clearly apparent, a characteristic that is generally considered undesirable. In contrast, sys2 does not display such an inverse response. Moreover, an examination of the crossover frequencies reveals that sys1's crossover frequency is 0.1491, approximately half that of sys2's, which is 0.2734.

From the example above, it becomes clear that explicitly considering the presence of RHP zeros in the control architecture design framework is essential. One approach to address this issue is to include a specific criterion for RHP zeros as an additional objective in the multi-objective optimization problem. Alternatively, RHP zeros can be treated as carefully imposed constraints. By incorporating these measures, we can minimize the negative effects of RHP zeros, leading to more robust and effective control architectures.

Controllability ensures the possibility of reaching any state x_1 by time $t_1 > t_0$. Nevertheless, achieving x_1 at t_1 might demand inputs that exceed practical constraints — in practice, input variables are typically limited. Additionally, substantial deviations in states or output variables may arise during the process of reaching x_1, and these variables might also be subject to practical constraints. It's important to recognize that the proposed framework does not address these constraints.

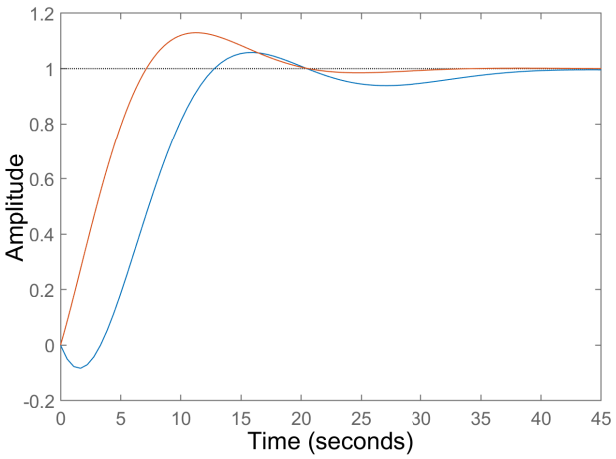

Figure 6: Step responses of the PI control systems sys1 (blue) and sys2 (red)

Another limitation of the proposed framework is that we have not incorporated considerations for uncertainty. In practice, uncertain models and measurements are common and carry significant implications, particularly in oil fields whose dynamics vary over time. Uncertainty arises from diverse sources, including equipment accuracy, measurement noise, unmodeled system dynamics, simplifying assumptions such as approximating nonlinear systems with linear ones, and parametric uncertainties, whether constant or time-varying. Notably, critical parameters such as gas to oil ratio, water cut, and productivity index introduce uncertainty in oil and gas production systems. Neglecting these uncertainties may impact the reliability of the identified optimal architecture, potentially resulting in it falling short of performance requirements. Rectifying design flaws post-implementation can incur prohibitively high costs, particularly in oil and gas production. Hence, it is imperative to account for uncertainties in the design of control architecture. Despite its importance, only a handful of studies have tried to tackle this problem. Recent studies include Yang et al. (2018), proposing an optimal sensor placement method for structural health monitoring systems, and Li et al. (2015), proposing an actuator placement method for active control system with uncertainties. Both studies use the interval analysis method to handle uncertainties.

5. Conclusions

In the context of oil and gas production plants, stakeholders want to achieve two interrelated but potentially contradictory objectives: maximizing plant performance and minimizing the cost of control equipment. In this study, we set out to develop a framework for optimal control architecture design that considers both of these objectives simultaneously. We formulated two multi-objective integer nonlinear programming problems — one for sensor selection and the other for actuator selection — considering observability and controllability as key performance criteria. Although it is possible to combine the two problems, they were treated separately in this study. The solutions to these optimization problems using a genetic algorithm (GA) lead to identification of Pareto-optimal control architectures, which allow design engineers to explore optimal trade-offs between cost and performance.

The presented framework was applied to a gas-lifted oil field model featuring two oil wells; four possible manipulated variables and twelve potential measured variables were present. To evaluate the impact of different control architectures on closed-loop control performance, we employed linear quadratic Gaussian (LQG) control design. LQG controllers were designed based on the Pareto-optimal control architectures and non-optimal architectures for comparison. The system responses were evaluated in terms of their settling times. Our analysis led to the following key observations:

- Control architecture significantly influences system performance.
- Several potential measured variables consistently appeared in nearly all identified optimal solutions, highlighting the need for physical sensors for these specific variables.
- A well-balanced distribution of sensors between oil wells is important.
- Introducing more sensors beyond the "critical" ones leads to diminished performance gains.
- Simultaneous actuation of the production valve alongside the gas-lift valve does not contribute to enhanced performance.

This research has established the foundational framework for further exploration of the control architecture design problem for oil and gas production systems. Future research avenues could include:

- Enhancing the actuator selection approach by incorporating specific criteria to address bandwidth limitations.
- Introducing a performance criterion that is more "directly" comparable to the cost of equipment. For example, quantifying the extent to which the setpoint can approach a hard constraint offers a more direct comparison to equipment costs than conventional measures of controllability or observability.
- Incorporating considerations for uncertainties within the framework, leading to more robust control architectures.
- Incorporating considerations for practical constraints in system variables.

Our paper contributes to the field of oil and gas production by advocating for a paradigm shift in control architecture design process. Specifically, we highlight the imperative for a more holistic approach, integrating both performance and cost considerations. The key contribution lies in bringing into perspective several distinct yet related metrics to achieve this holistic perspective. In essence, our research propels the advancement of control system design in the oil and gas industry, offering valuable insights that can be applied to address similar challenges in other complex processes.

Acknowledgments

We gratefully acknowledge the economic support from The Research Council of Norway and Equinor ASA through Research Council project "308817 - Digital wells for optimal production and drainage" (DigiWell).

References

Antoniades, C. and Christofides, P. D. Computation of optimal actuator locations for nonlinear controllers in transport-reaction processes. *Computers & Chemical Engineering*, 2000. 24(2-7):577–583. doi:10.1016/S0098-1354(00)00412-9.

Bruant, I., Gallimard, L., and Nikoukar, S. Optimal piezoelectric actuator and sensor location for active vibration control, using genetic algorithm. *Journal of Sound and Vibration*, 2010. 329(10):1615–1635. doi:10.1016/j.jsv.2009.12.001.

Cha, Y.-J., Agrawal, A. K., Kim, Y., and Raich, A. M. Multi-objective genetic algorithms for cost-effective distributions of actuators and sensors in large structures. *Expert Systems with Applications*, 2012. 39(9):7822–7833. doi:10.1016/j.eswa.2012.01.070.

Darivandi, N., Morris, K., and Khajepour, A. An algorithm for LQ optimal actuator location. *Smart Materials and Structures*, 2013. 22(3):035001. doi:10.1088/0964-1726/22/3/035001.

Doyle, J. and Stein, G. Robustness with observers. *IEEE Transactions on Automatic Control*, 1979. 24(4):607–611. doi:10.1109/TAC.1979.1102095.

Doyle, J. and Stein, G. Multivariable feedback design: Concepts for a classical/modern synthesis. *IEEE Transactions on Automatic Control*, 1981. 26(1):4–16. doi:10.1109/TAC.1981.1102555.

Flynn, E. B. and Todd, M. D. A Bayesian approach to optimal sensor placement for structural health monitoring with application to active sensing. *Mechanical Systems and Signal Processing*, 2010. 24(4):891–903. doi:10.1016/j.ymssp.2009.09.003.

Georges, D. The use of observability and controllability gramians or functions for optimal sensor and actuator location in finite-dimensional systems. In *Proceedings of 1995 34th IEEE Conference on Decision and Control*, volume 4. IEEE, New Orleans, LA, USA, pages 3319–3324, 1995. doi:10.1109/CDC.1995.478999.

Goldberg, D. E. *Genetic Algorithms in Search, Optimization, and Machine Learning*. Addison-Wesley Pub. Co, Reading, Mass, 1989.

Goodwin, G. C., Graebe, S. F., Salgado, M. E., and Goodwin, G. C. *Control System Design*. Prentice Hall, Upper Saddle River, NJ, 2001.

Hać, A. and Liu, L. Sensor And Actuator Location In Motion Control Of Flexible Structures. *Journal of Sound and Vibration*, 1993. 167(2):239–261. doi:10.1006/jsvi.1993.1333.

Hiramoto, K., Doki, H., and Obinata, G. Optimal sensor/actuator placement for active vibration control using explicit solution of algebraic Riccati equation. *Journal of Sound and Vibration*, 2000. 229(5):1057–1075. doi:10.1006/jsvi.1999.2530.

Jayamanne, K. R. *Optimal Operation of Processes Under Uncertainty Using Robust Model Predictive Control*. Ph.D. thesis, University of South-Eastern Norway, 2021. URL https://hdl.handle.net/11250/2765105.

Kookos, I. K. and Perkins, J. D. A Systematic Method for Optimum Sensor Selection in Inferential Control Systems. *Industrial & Engineering Chemistry Research*, 1999. 38(11):4299–4308. doi:10.1021/ie9902737.

Leleu, S., Abou-Kandil, H., and Bonnassieux, Y. Piezoelectric actuators and sensors location for active control of flexible structures. In *Proceedings of the 17th IEEE Instrumentation and Measurement Technology Conference [Cat. No. 00CH37066]*, volume 2. IEEE, Baltimore, MD, USA, pages 818–823, 2000. doi:10.1109/IMTC.2000.848848.

Li, Y., Wang, X., Huang, R., and Qiu, Z. Actuator placement robust optimization for vibration control system with interval parameters. *Aerospace Science and Technology*, 2015. 45:88–98. doi:10.1016/j.ast.2015.04.017.

Lie, B. Attainable Performance in LQG Control. In R. Berber, editor, *Methods of Model Based Process Control*, pages 263–295. Springer Netherlands, Dordrecht, 1995. doi:10.1007/978-94-011-0135-6_11.

Lim, K. B. Method for optimal actuator and sensor placement for large flexible structures. *Journal of Guidance, Control, and Dynamics*, 1992. 15(1):49–57. doi:10.2514/3.20800.

Luyben, M. and Floudas, C. Analyzing the interaction of design and control—1. A multiobjective framework and application to binary distillation synthesis. *Computers & Chemical Engineering*, 1994. 18(10):933–969. doi:10.1016/0098-1354(94)E0013-D.

Ma, Y., Gowda, S., Anantharaman, R., Laughman, C., Shah, V., and Rackauckas, C. ModelingToolkit: A Composable Graph Transformation System For Equation-Based Modeling. 2021. doi:10.48550/ARXIV.2103.05244.

Manohar, K., Brunton, B. W., Kutz, J. N., and Brunton, S. L. Data-Driven Sparse Sensor Placement for Reconstruction: Demonstrating the Benefits of Exploiting Known Patterns. *IEEE Control Systems*, 2018. 38(3):63–86. doi:10.1109/MCS.2018.2810460.

Manohar, K., Kutz, J. N., and Brunton, S. L. Optimal Sensor and Actuator Selection Using Balanced Model Reduction. *IEEE Transactions on Automatic Control*, 2022. 67(4):2108–2115. doi:10.1109/TAC.2021.3082502.

Milosevic, B. and Begovic, M. Nondominated sorting genetic algorithm for optimal phasor measurement placement. *IEEE Transactions on Power Systems*, 2003. 18(1):69–75. doi:10.1109/TPWRS.2002.807064.

Mitchell, M. *An Introduction to Genetic Algorithms*. The MIT Press, 1998. doi:10.7551/mitpress/3927.001.0001.

Müller, P. and Weber, H. Analysis and optimization of certain qualities of controllability and observability for linear dynamical systems. *Automatica*, 1972. 8(3):237–246. doi:10.1016/0005-1098(72)90044-1.

Munz, U., Pfister, M., and Wolfrum, P. Sensor and Actuator Placement for Linear Systems Based on H_2 and H_∞ Optimization. *IEEE Transactions on Automatic Control*, 2014. 59(11):2984–2989. doi:10.1109/TAC.2014.2351673.

Muske, K. R. and Georgakis, C. Optimal measurement system design for chemical processes. *AIChE Journal*, 2003. 49(6):1488–1494. doi:10.1002/aic.690490612.

Paris, R., Beneddine, S., and Dandois, J. Reinforcement-learning-based actuator selection method for active flow control. *Journal of Fluid Mechanics*, 2023. 955:A8. doi:10.1017/jfm.2022.1043.

Pequito, S., Kar, S., and Aguiar, A. P. A Framework for Structural Input/Output and Control Configuration Selection in Large-Scale Systems. *IEEE Transactions on Automatic Control*, 2016. 61(2):303–318. doi:10.1109/TAC.2015.2437525.

Semaan, R. Optimal sensor placement using machine learning. *Computers & Fluids*, 2017. 159:167–176. doi:10.1016/j.compfluid.2017.10.002.

Sen, P., Sen, K., and Diwekar, U. M. A multi-objective optimization approach to optimal sensor location problem in IGCC power plants. *Applied Energy*, 2016. 181:527–539. doi:10.1016/j.apenergy.2016.08.006.

Sharma, R., Fjalestad, K., and Glemmestad, B. Modeling and control of gas lifted oil field with five oil wells. In *52nd International Conference of Scandinavian Simulation Society, SIMS*. pages 29–30, 2011.

Skogestad, S. and Wolff, E. A. Controllability measures for disturbance rejection. *Modeling, Identification and Control: A Norwegian Research Bulletin*, 1996. 17(3):167–181. doi:10.4173/mic.1996.3.1.

Stein, G. and Athans, M. The LQG/LTR procedure for multivariable feedback control design. *IEEE Transactions on Automatic Control*, 1987. 32(2):105–114. doi:10.1109/TAC.1987.1104550.

Summers, T. H. and Lygeros, J. Optimal Sensor and Actuator Placement in Complex Dynamical Networks. *IFAC Proceedings Volumes*, 2014. 47(3):3784–3789. doi:10.3182/20140824-6-ZA-1003.00226.

Van De Wal, M. and De Jager, B. A review of methods for input/output selection. *Automatica*, 2001. 37(4):487–510. doi:10.1016/S0005-1098(00)00181-3.

Yang, C., Lu, Z., and Yang, Z. Robust optimal sensor placement for uncertain structures with interval parameters. *IEEE Sensors Journal*, 2018. 18(5):2031–2041. doi:10.1109/JSEN.2018.2789523.

A. Linearized Oil Field Model

The nonlinear oil field model presented by Jayamanne (2021) was linearized around the following operating point:

$$x_0 = \begin{bmatrix}1.8208, 1.1773, 2.2191, 1.7053, 1.1492, 1.9696\end{bmatrix},$$
$$u_0 = \begin{bmatrix}4.1500, 30.0000, 4.1500, 30.0000\end{bmatrix}.$$

The following ranges were used to normalize the linearized model:

$$\begin{bmatrix}x_{\min} & x_{\max}\end{bmatrix} = \begin{bmatrix}1.4580 & 2.1823\\ 1.1622 & 1.2321\\ 2.1530 & 2.2540\\ 1.3648 & 2.0445\\ 1.1321 & 1.1970\\ 1.9057 & 2.0119\end{bmatrix},$$

$$\begin{bmatrix}u_{\min} & u_{\max}\end{bmatrix} = \begin{bmatrix}3.4583 & 4.8417\\ 25.0000 & 30.0000\\ 3.4583 & 4.8417\\ 25.0000 & 30.0000\end{bmatrix},$$

$$\begin{bmatrix}y_{\min} & y_{\max}\end{bmatrix} = \begin{bmatrix}459.37 & 687.58\\ 526.98 & 788.78\\ 129.94 & 132.51\\ 33.45 & 34.96\\ 3.46 & 4.84\\ 63.71 & 83.30\\ 463.44 & 694.26\\ 533.84 & 799.72\\ 128.24 & 131.74\\ 32.94 & 34.22\\ 3.46 & 4.84\\ 58.74 & 76.28\end{bmatrix}.$$

The state space model matrices of the normalized oil field model are as follows:

$$A = \begin{bmatrix} -0.0002 & 0 & 0 & 0 & 0 & 0 \\ 0.0200 & -0.0385 & -0.0234 & 0 & 0 & 0 \\ 0 & -0.0808 & -0.0870 & 0 & 0 & 0 \\ 0 & 0 & 0 & -0.0002 & 0 & 0 \\ 0 & 0 & 0 & 0.0216 & -0.0460 & -0.0296 \\ 0 & 0 & 0 & 0 & -0.0650 & -0.0704 \end{bmatrix},$$

$$B = \begin{bmatrix} 0.0002 & 0 & 0 & 0 \\ 0 & -0.0099 & 0 & 0 \\ 0 & -0.0129 & 0 & 0 \\ 0 & 0 & 0.0002 & 0 \\ 0 & 0 & 0 & -0.0107 \\ 0 & 0 & 0 & -0.0112 \end{bmatrix},$$

$$C = \begin{bmatrix} 1.0000 & 0 & 0 & 0 & 0 & 0 \\ 1.0000 & 0 & 0 & 0 & 0 & 0 \\ 0 & 1.9538 & 2.9475 & 0 & 0 & 0 \\ 0 & 3.1259 & 2.2228 & 0 & 0 & 0 \\ 1.0090 & 0.0178 & 0.0268 & 0 & 0 & 0 \\ 0 & 2.5143 & 1.8743 & 0 & 0 & 0 \\ 0 & 0 & 0 & 1.0000 & 0 & 0 \\ 0 & 0 & 0 & 1.0000 & 0 & 0 \\ 0 & 0 & 0 & 0 & 1.3538 & 2.3496 \\ 0 & 0 & 0 & 0 & 3.4518 & 2.5670 \\ 0 & 0 & 0 & 1.0124 & 0.0168 & 0.0292 \\ 0 & 0 & 0 & 0 & 2.8832 & 2.2484 \end{bmatrix},$$

$$D = \begin{bmatrix} 0 & 0 & 0 & 0 \\ 0 & 0 & 0 & 0 \\ 0 & 0 & 0 & 0 \\ 0 & 0 & 0 & 0 \\ 0 & 0 & 0 & 0 \\ 0 & 0.7009 & 0 & 0 \\ 0 & 0 & 0 & 0 \\ 0 & 0 & 0 & 0 \\ 0 & 0 & 0 & 0 \\ 0 & 0 & 0 & 0 \\ 0 & 0 & 0 & 0 \\ 0 & 0 & 0 & 0.7152 \end{bmatrix}.$$